A 135–150-GHz Frequency Tripler Using SU-8 Micromachined WR-5 Waveguides

Cheng Guo, Yuvaraj Dhayalan, Xiaobang Shang, *Senior Member, IEEE*, Jeffrey Powell, Michael J. Lancaster, *Senior Member, IEEE*, Jun Xu, Yi Wang, *Senior Member, IEEE*, Hui Wang, Byron Alderman, and Peter G. Huggard, *Senior Member, IEEE*

***Abstract*— This article presents a 135–150-GHz Schottky diode-based bias-less frequency tripler based on SU-8 micromachined WR-5 waveguides. The waveguides consist of five 432-μm-thick silver-plated SU-8 layers, which house the diode chip and form the output matching network. The input matching circuit is realized in a computer numerical control (CNC) milled waveguide filter, which also provides support and thermal sink to the SU-8 waveguides. Considering the low thermal conductivity of the SU-8 material, auxiliary metallic thermal paths are designed, and the impact of these is discussed through thermal modeling. The thermal simulations show that under 50-mW power dissipation in the diode anodes, the maximum temperature of the SU-8 tripler is predicted to be 346 K at the diode junction, only 7 K higher than in an entirely metal equivalent. The tripler was measured to have a conversion loss of 16–18 dB and the input return loss is better than 18 dB. This work demonstrates that SU-8 micromachined waveguides can be used to package high-frequency semiconductor components, which, like other photolithography-based processes such as silicon deep reactive ion etching (Si-DRIE), has the potential for submicrometer feature resolution.**

***Index Terms*— Filter matching, multiplier, planar Schottky diodes, SU-8 waveguide.**

I. Introduction

In THE past few decades, millimeter and terahertz (THz) waves have been found very useful in applications such as imaging [1]–[3], high-speed communication [4], [5], remote sensing [6], and spectroscopy [7], [8]. At this frequency band, air-filled waveguide is widely adopted as the basic building block for a wide range of devices. Conventional metal machining techniques, such as computer numerical control (CNC) milling, have been successfully used to fabricate waveguide structures up to several THz [9]. However, as the frequency increases, the dimensions of the waveguide structures decrease, and the fabrication becomes more expensive and time consuming. Apart from CNC milling, several photolithography-based micromachining technologies have been reported to be capable of not only producing 3-D structures with high accuracy and large aspect ratio but also of facilitating large-scale inexpensive fabrication. These techniques include silicon deep reactive ion etching (Si-DRIE) [10], [11], LIthographie, Galvanoformung and Abformung (LIGA) [12], metal electroforming [13], [14], and SU-8 photoresist technology [15]–[20]. A wide range of passive devices, with excellent performance, have been demonstrated using these micromachining techniques [19].

Demonstration of circuits containing active semiconductor components has been reported using electroforming and Si-DRIE micromachined waveguides. A G-band (140–220 GHz) power combining amplifier with 16 waveguide channels [14] delivered state-of-the-art output power of 820 mW. In [21] and [22], Schottky diode-based frequency multipliers and mixers were packaged using Si-DRIE waveguides formed of multiple micromachined layers. Based on the same technology, compact systems, including both passive and active components, have been integrated, such as the 8-pixel 340-GHz image radar in [23] and the 560-GHz sideband separation receiver in [24]. The measured performance of these micromachined devices and systems is similar to those packaged with CNC-milled metallic waveguide blocks.

To date, in contrast to Si-DRIE and the other demonstrators, reports of devices using SU-8 micromachining for passive components and have exhibited excellent performance [15]–[20]. For example, in our previous work, we have achieved an insertion loss as low as 0.048 and 0.031 dB/mm for WR-3 waveguides (220–325 GHz, waveguide dimensions: 0.864 mm × 0.432 mm) made from single- and double-deposition SU-8 layers, respectively [15]. This is comparable to the performance of milled and gold-plated metallic waveguide (0.021 dB/mm) [15]. Also, in [15], a fifth-order filter with 9% of bandwidth made using the same SU-8 processes has achieved an average

Manuscript received May 26, 2019; revised September 16, 2019; accepted November 8, 2019. Date of publication December 27, 2019; date of current version March 4, 2020. This work was supported in part by the U.K. Engineering and Physical Science Research Council (EPSRC) under Contract EP/M016269/1, in part by the China Postdoctoral Science Foundation under Grant 2019M663715, and in part by the Fundamental Research Funds for the Central Universities under Grant xxj032019001. *(Corresponding authors: Cheng Guo; Michael J. Lancaster.)*

C. Guo is with the School of Information and Communication Engineering, Xi'an Jiaotong University, Xi'an 710049, China, and also with the Department of Electronics, Electrical and Systems Engineering, University of Birmingham, Birmingham B15 2TT, U.K. (e-mail: spmguo@163.com).

Y. Dhayalan, M. J. Lancaster, and Y. Wang are with the Department of Electronics, Electrical and Systems Engineering, University of Birmingham, Birmingham B15 2TT, U.K. (e-mail: m.j.lancaster@bham.ac.uk).

X. Shang is with the National Physical Laboratory, Teddington TW11 0LW, U.K. (e-mail: shangxiaobang@gmail.com).

J. Powell is with Skyarna Ltd., West Midlands B63 3TT, U.K. (e-mail: jeff.powell@skyarna.com).

J. Xu is with the School of Physical Electronics, University of Electronic Science and Technology of China, Chengdu 610054, China (e-mail: xujun@uestc.edu.com).

H. Wang, B. Alderman, and P. G. Huggard are with RAL Space, STFC Rutherford Appleton Laboratory, Oxfordshire OX11 0QX, U.K. (e-mail: hui.wang@stfc.ac.uk; byron.alderman@stfc.ac.uk; peter.huggard@stfc.ac.uk).

Color versions of one or more of the figures in this article are available online at http://ieeexplore.ieee.org.

Digital Object Identifier 10.1109/TMTT.2019.2955684

2.2 dB (using single-deposition process) and 1.6 dB (using double-deposition process) insertion losses.

Considering the excellent performance of these SU-8 passive devices, integration of the SU-8 waveguides with the active semiconductor components is the next obvious step. An integrated micromachined frequency tripler based on heterostructure barrier varactor (HBV) diodes and SU-8 micromachined waveguides as the package of the HBV chip is presented in [25]. In this article, we present a Schottky diode-based, 135–150-GHz frequency tripler. As shown in Fig. 1, five micromachined and subsequently metalized SU-8 layers are used to create the WR-5 waveguide, with dimensions 1.296 mm × 0.648 mm [Fig. 1(b)]. Unlike the work in [25], in our work, the SU-8 not only forms the packaging for the diode chip but also the output impedance matching network and the output waveguide flange for the tripler. Input matching is achieved in a CNC machined metal waveguide filter, which is also used to support and to provide a thermal sink for the SU-8 layers. The whole structure is stabilized by a top metal plate, bolted through the SU-8 layers to the input waveguide filter, as shown in Fig. 1(c). Such a hybrid structure enables the advantages of both the CNC and the SU-8 to be fully utilized, as SU-8 can hardly be not sensibly be used to fabricate the WR-19 waveguide because it requires too many layers.

Because the thermal conductivity of SU-8 is much lower than metal, we also report on thermal designs and simulations performed to evaluate the steady-state temperature of this SU-8-based device under nominal power dissipation. The manufacturing, assembly, and test procedures are then described. The successful demonstration of tripler made from multiple SU-8 layers represents a substantial and comprehensive step forward in the development of SU-8 micromachined devices.

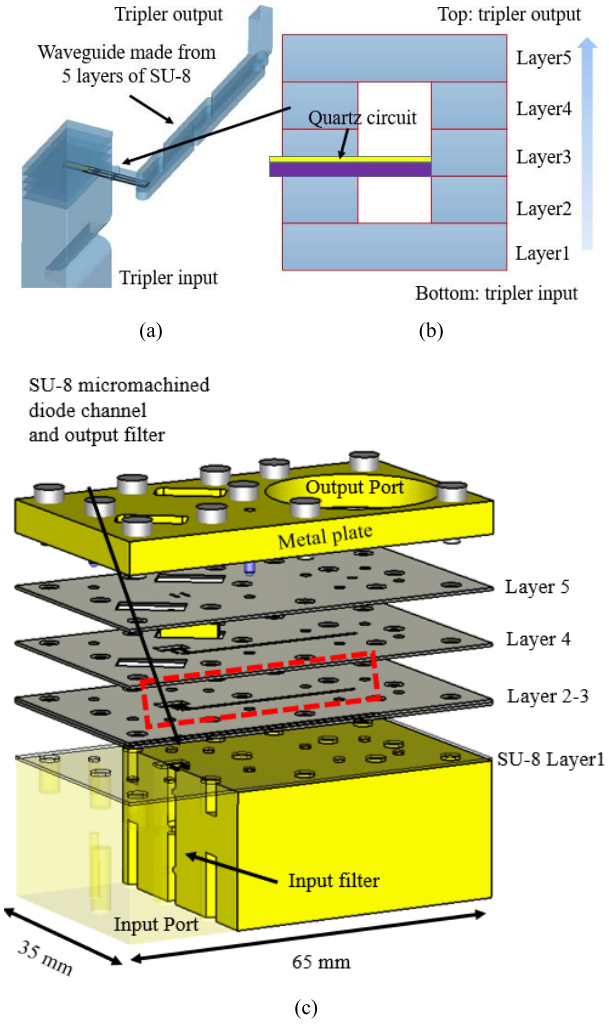

Fig. 1. Frequency tripler fabricated by SU-8 micromachining. (a) 3-D model of the tripler. (b) Cross-sectional view of the WR-5 waveguide, 1.296 mm × 0.648 mm, made from five 432-μm-thick layers of SU-8. (c) Exploded model of the tripler. The CNC machined metal parts are represented using yellow color and the SU-8 layers are shown as gray color.

II. Tripler Design and Thermal Considerations

In this work, the impedance matching of the diode chip is realized by waveguide filters using a coupled resonator design methodology [26], [27]. The circuit configuration is shown diagrammatically in Fig. 2. The input and output of the diode chip are directly coupled to the 3rd and 4th waveguide resonators. The two resonators belong to the input and output filters, respectively. Coupled resonator filters were successfully used as impedance matching networks for a wide range of devices such as mixers [26], frequency multipliers [27], and amplifiers [28]–[33], from a few gigahertzes to 300 GHz. One advantage is the compact circuit size with filtering, matching, and the waveguide to microstrip (MS) transition to be realized in one structure. The other benefit is that lower loss can be achieved, as most of the matching elements were moved from the MS circuit into the waveguide resonators [26], [27]. The detailed design procedure of the triplers is given in Section II-A.

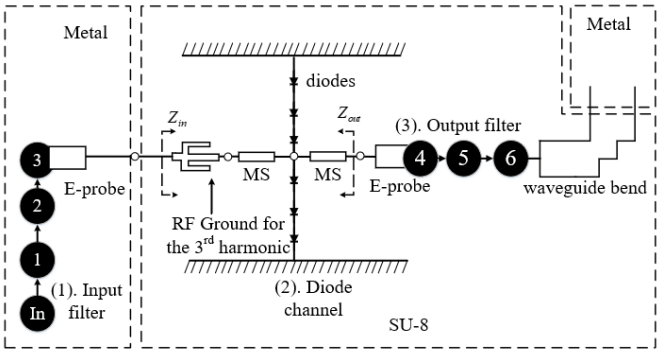

Fig. 2. Input and output matching realized using waveguide resonators (black filled circles). The input and output of the diodes are coupled via an MS line and E-plane probe to the 3rd, in CNC waveguide, and the 4th, in SU-8 waveguide, resonators.

A. SU-8 Tripler Design

A Schottky diode monolithic microwave integrated circuit (MMIC) (Teratech components Ltd SC6/6G2/16p3, operating in a biasless varistor mode) was used as the core part of the tripler. The MMIC was flip-chip soldered onto a 50-μm-thick quartz thin-film circuit, which is placed between the 2nd and 3rd SU-8 layers [hence, the two layers are shown as one piece in Fig. 1(c)]. The enlarged view of the diode

TABLE I
DIODE PARAMETERS AND MMIC INPUT–OUTPUT IMPEDANCES

R_s	n	I_s	C_{j0}	Z_{in}(A)	Z_{out}(A)	Z_{in}(M)	Z_{out}(M)
2Ω	1.2	1.5fA	24.2fF	79-j12	38-j14	28+j5	67-j15

R_s: Series resistance; n: Ideality factor; I_s: Saturation current; C_{j0}: Nonlinear junction capacitance at zero bias voltage; "A" indicates the anode impedance, while "M" is for MMIC impedance. All impedances are at the centre frequency ("in" is for input impedance at 47.5GHz and "out" is for output impedance at 142.5 GHz.), and a 10-Ω impedance is presented to the higher harmonics.

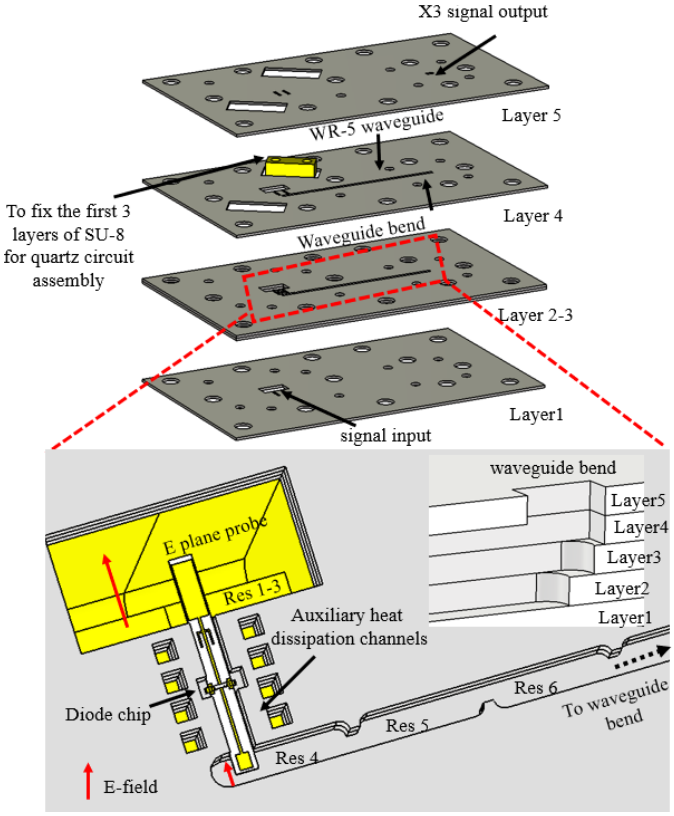

Fig. 3. Tripler without the CNC part, including the SU-8 micromachined diode channel and WR-5 output waveguide. Only the 2nd and 3rd SU-8 layers and the input waveguide are enlarged and shown in the bottom part of the diagram. Inset: approach used in the SU-8 layers to achieve the 90° H-plane bend to the output port.

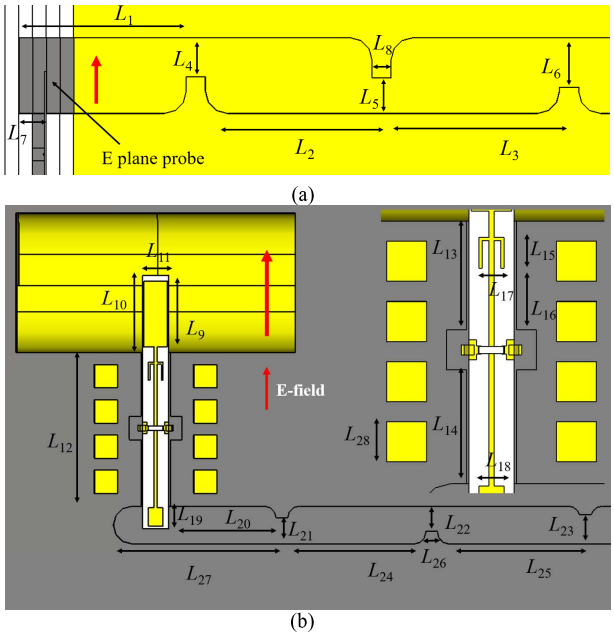

Fig. 4. SU-8 tripler design. (a) Input filter. (b) Quartz circuit and the output filter (the quartz circuit is enlarged). Some critical dimensions are (in millimeters). $L_1 = 4.851$, $L_2 = 5.257$, $L_3 = 5.314$, $L_4 = 1.232$, $L_5 = 1.117$, $L_6 = 1.562$, $L_7 = 0.864$, $L_8 = 0.600$, $L_9 = 1.119$, $L_{10} = 1.319$, $L_{11} = 0.600$, $L_{12} = 2.620$, $L_{13} = 1.084$, $L_{14} = 1.132$, $L_{15} = 1.305$, $L_{16} = 0.616$, $L_{17} = L_{18} = 0.250$, $L_{19} = 0.338$, $L_{20} = 1.833$, $L_{21} = 0.448$, $L_{22} = 0.431$, $L_{23} = 0.497$, $L_{24} = 2.732$, $L_{25} = 2.431$, $L_{26} = 0.200$, $L_{27} = 2.782$, and $L_{28} = 0.400$.

channel is shown in Fig. 3. The input signal is fed from a CNC-milled, WR-19 waveguide via an E-plane probe to the diode chip. The generated 3rd harmonic is coupled to the WR-5 output waveguide via another E-plane probe. An H-plane waveguide bend, shown in the inset in Fig. 3, is used to redirect the signal perpendicular to the plane of the output flange. The simulated return loss for the bend is better than 20 dB across the entire WR-5 band. Additional auxiliary heat conduction channels (square silver-coated holes in the SU-8 layers) were added near the diode chip to mitigate the relatively poor thermal conductivity of the SU-8 material compared to the metal used in the auxiliary conduction channels.

To design the input and output matching filters, the procedure discussed in [27] has been used: The tripler was designed to have an input power of 50 mW and output frequency centered at 142.5 GHz with a bandwidth of 15 GHz. A third-order Chebyshev response with 20-dB passband return loss was used to impedance match the impedance Z_{out} of the diode chip. Similarly, a third-order filter centered at 47.5 GHz with 5-GHz bandwidth was used to match the input. The two filters share the same coupling matrix and the resulting nonzero coupling coefficients m_{ij} and external quality factors Q_e are $m_{12} = m_{23} = 0.108$ and $Q_{e1} = Q_{e3} = 8.09$ [34].

To match directly the impedance of the diode MMIC using the filters, the embedding impedances of the diode chip at the input and output frequencies, namely, Z_{in} and Z_{out} are required. A nonlinear diode model, together with the S-parameters of the diode package, was used in an ADS harmonic balance simulator to determine the optimum input–output embedding impedances at 45–50 GHz and 135–150 GHz, respectively. The diode parameters are listed in Table I, together with the obtained impedances from ADS. It should be noted that the impedances are frequency (and power) dependent and only the value at the center frequency is listed here. The non-50-Ω impedances obtained can be

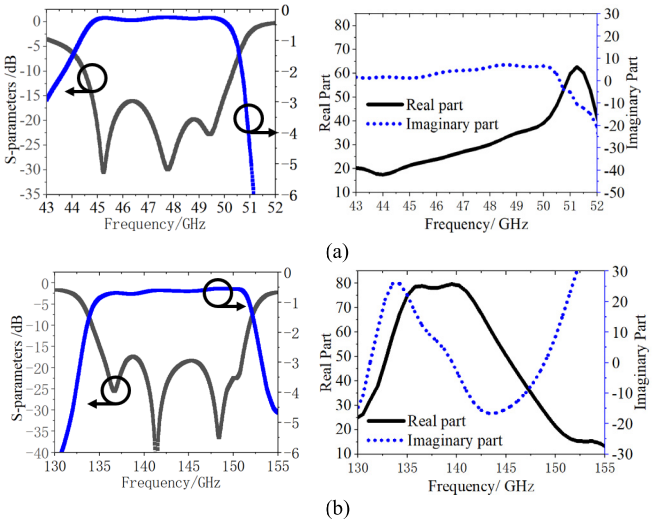

Fig. 5. Performance of the input and output filters with the complex impedance load. (a) Input filter and the input impedance. (b) Output filter (including the waveguide bend) and the output impedance.

directly matched within the filters, as discussed in [27]. The 3-D modeling, full-wave simulation and optimization of the impedance matching filters were done in CST, and the obtained physical dimensions are shown in Fig. 4. Fig. 5 shows the optimized filter performance, including the frequency-dependent complex loads (also shown in Fig. 5), at 43–52 GHz and 130–155 GHz. After the filters were designed, the filters and the diode MMIC were combined and simulated in ADS, and the tripler performance was then estimated. For under 50-mW input power, the simulated input and output return losses are all better than 18 dB at the output frequencies of 135–150 GHz. The simulated conversion loss is approximately 13 dB, corresponding to an efficiency of 5%.

B. Thermal Considerations

The thermal conductivity of the SU-8 photoresist used in this work is 0.2 W/(K·m), about three orders of magnitude lower than brass. The biasless diode used in this design results in 95% of the input power being converted into heat. Therefore, the heat dissipation of the tripler must be considered. The 3-D model of the diode chip and its surrounding package, together with the equivalent thermal circuit schematics, are shown in Fig. 6. Note that in Fig. 6(b), there are four circuit models in total, corresponding to different material settings and this will be detailed later in this section. The use of the thermal circuit is valid as the heat conduction problem in the passive region satisfies the Laplace equation. Hence, the governing equations are identical to the electrostatic problem [35]. Therefore, a thermal circuit model can be constructed by analogy to the electric circuit model. The thermal resistance is defined by

$$R = L/\sigma S \tag{1}$$

where L, S, and σ represent for the length, the cross section area, and the thermal conductivity of the material. In the equivalent thermal circuits shown Fig. 6, T_s represents the temperature of the heat source, i.e., the Schottky junction,

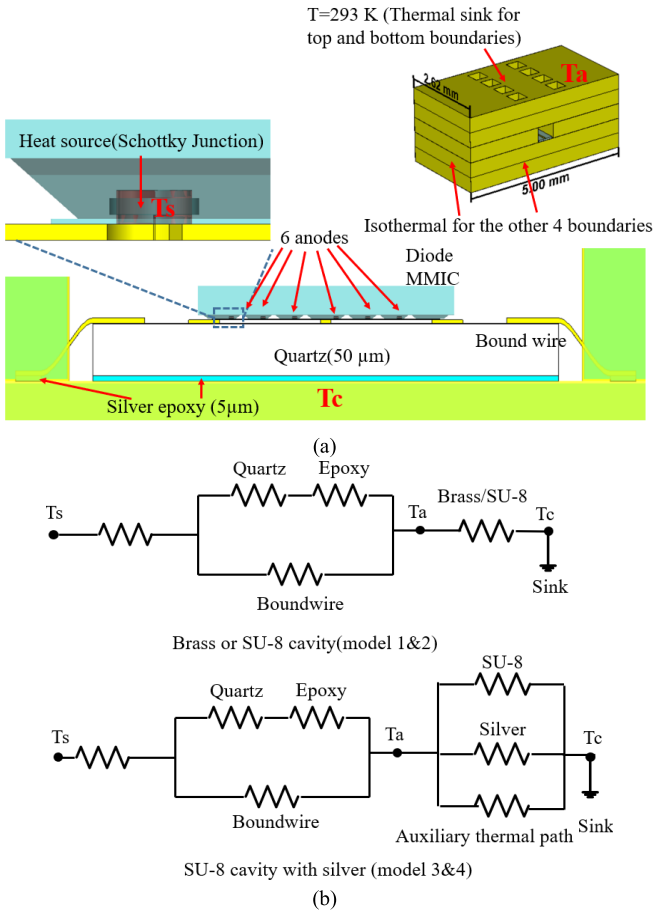

Fig. 6. 3-D model and the equivalent thermal circuits for the Schottky diodes in SU-8 and metal cavities. (a) 3-D model. (b) Equivalent thermal circuit modes.

while T_a is the ambient temperature, 293 K. From the source to the sink, the heat flows through the package of the diode MMIC and continues to propagate via the quartz substrate (and the silver epoxy) in parallel with the gold bond-wire to the SU-8, at temperature T_c(the location is chosen to be below the center of the MMIC). The heat is then conducted through the SU-8 layers to the metal part of the tripler at ambient temperature T_a.

To find T_s, T_c, and the thermal resistances of the tripler, CST thermal solver can be used and the dissipated power is represented by placing heat sources at each of the diode anode positions [36]. The heat source power is set to be 50 mW (in order to simulate the worst condition, that all the input power is converted to heat) and it is equally distributed to the six anodes. To reduce the simulation time, only a section of the tripler was used in the CST simulation, the length of the section is chosen to be 2.62 mm, which is the same with the diode channel shown in Fig. 4, and the width is chosen to be 5 mm. Because the SU-8 layers are sandwiched between the input metal filter and the output brass plate, hence, the top and bottom boundary conditions are chosen to be with constant ambient temperature T_a. For the other four boundaries, the isothermal boundary condition was used, as shown in Fig. 6(a). The thermal conductivities of the materials used in the simulations are listed in Table II.

TABLE II
THERMAL CONDUCTIVITIES OF THE MATERIALS USED IN SIMULATION

GaAs	Brass	Silver	SU-8	Quartz	Gold	Epoxy
54	120	429	0.2	1.4	314	29

*Units are W/K/m.

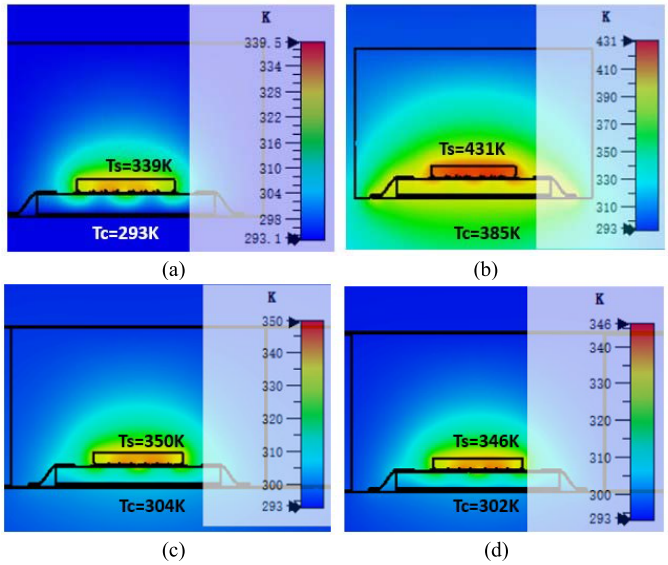

Fig. 7. Simulation results of the temperature distribution along the diode MMIC for several different materials: (a) brass, (b) SU-8, (c) SU-8 with 2-μm silver plating, and (d) SU-8 with 2-μm silver plating and the auxiliary thermal paths.

In order to find a good thermal solution for SU-8 waveguide devices, four models were considered, and their thermal circuits are shown in Fig. 6(b). Note that the thermal circuits are not used to calculate anything but to identify the different material settings in these models. The first two models use brass or SU-8 (without silver) in the CST thermal simulation. The steady-state temperature distributions along the six-anode MMIC are shown in Fig. 7(a) and (b), and the results are summarized in Table III. The thermal resistance for the brass cavity is almost zero, whereas the resistance for the SU-8 cavity is 1.84 K/mW. The last two models both use 2-μm-thick silver-plated SU-8 in the thermal simulation but differ in the existence of the auxiliary thermal paths in the 4th model. The simulated temperature distributions are shown in Fig. 7(c) and (d) and the calculated thermal resistances are 0.22 and 0.18 K/mW, respectively. Again, the simulated thermal performance for the last two models is summarized in Table III. As a result, for 50 mW of heat power, the maximum temperature for the four models is 339, 431, 350, and 346 K, respectively.

In summary, the thermal simulations show that silver-plated SU-8 can be used for this tripler design. The thermal resistance of the proposed silver-coated structure with auxiliary thermal paths is 0.18 K/mW and is much better than the 1.84 K/mW of pure SU-8. Under 50-mW thermal power, the maximum temperature at the core of the diode junction is only raised by 7 K compared with the case packaged with the brass cavity. If more power needs to be handled, better thermal design can be used by adding more thermal paths in the SU-8 layers.

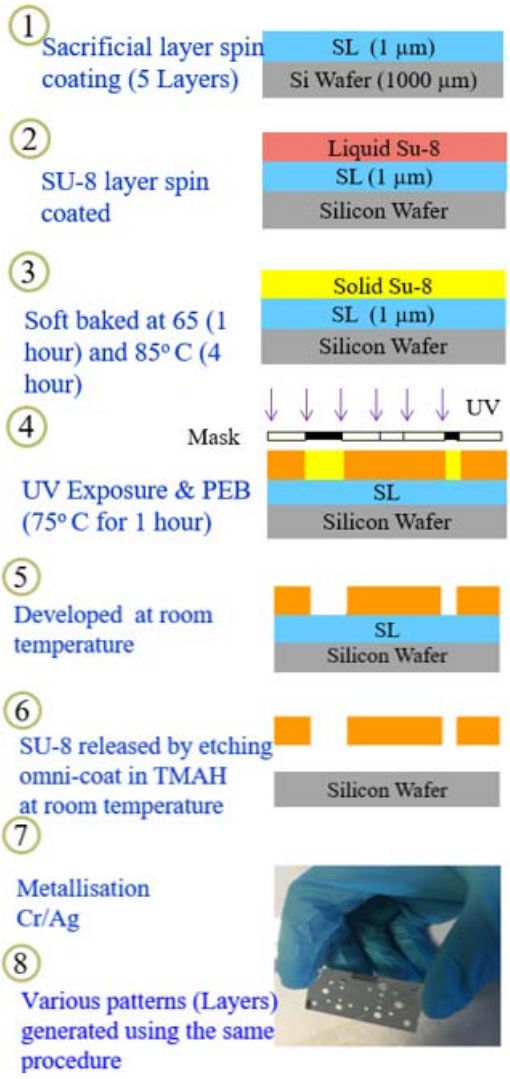

Fig. 8. Single-layer SU-8 process used in this work. SL: sacrificial layer; TMAH:$C_4H_{13}NO$. PEB: post exposure bake.

III. FABRICATION AND ASSEMBLY

For the SU-8 tripler, the input filter was CNC machined from aluminum with the block split in the E-plane. The top metal plate was machined from brass. The SU-8 layers were micromachined using a single deposition process (namely, fabricate only one SU-8 layer at a time), as illustrated in Fig. 8. The fabrication process is like the one used in [15], except that in step 1, an additional 1-μm-thick sacrificial layer was added between the silicon handle wafer and the SU-8 to facilitate the release process. The layer thickness was chosen to be 432 μm to be consistent with the well-developed process used to fabricate the WR-3 waveguide devices in the past (see [15], [16]).

The assembly of the tripler is illustrated in Fig. 9 and it consists of six steps as follows:

1) The kit of component parts is collected [see Fig. 9(d)].
2) Two precision alignment pins are inserted into the metal lower block, and the SU-8 layers 1–3 are positioned using the pins. Note that layers 2 and 3 constitute the diode channel.

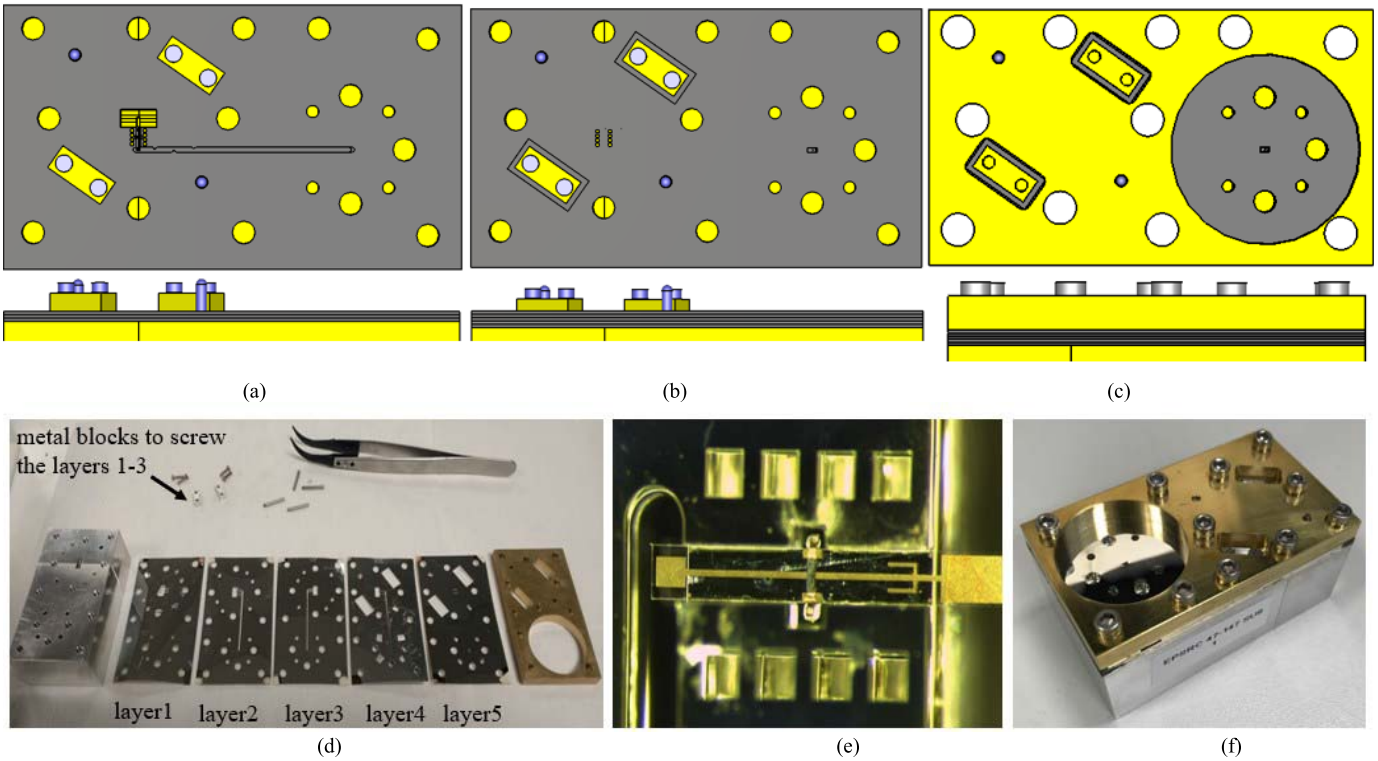

Fig. 9. Tripler before and after assembly. (a)–(c) Assembly process. (d) and (e) Metal parts and SU-8 layers before assembly and tripler with the layers 1–3 and the quartz circuit assembled, respectively. (f) Tripler after assembly.

TABLE III
THERMAL RESISTANCES OBTAINED AT DIFFERENT JUNCTIONS OF THE THERMAL CIRCUIT

Model	Ts (K)	Tc (K)	Rsc (K/mW)	Rca (K/mW)	Rsa (K/mW)
Brass	339	293	0.92	≈ 0	0.92
SU-8 only	431	385	0.92	1.84	2.76
Silver coated SU-8	350	304	0.92	0.22	1.14
Silver coated SU-8 with auxiliary thermal paths	346	302	0.88	0.18	1.06

*Rsc represents the thermal resistance between Ts and Tc, Rca is for the thermal resistance between Tc and Ta, Rsa is the total resistance of the structure (hence we have Rsa = Rsc + Rca.) The unit for temperature is K, for thermal resistance this is K/mW.

3) These three SU-8 layers are fixed tightly on the lower block using two small metal clamp blocks.
4) The quartz circuit with the flip-chip soldered diode is inserted into the channel, and gold bond wire and silver loaded epoxy are used to ground the diode chip. This step is shown in Fig. 9(a). The enlarged view can be found in Figs. 3 and 9(e).
5) The 4th and 5th SU-8 layers are placed on top of layer 3 [see Fig. 9(b)].
6) The brass plate is placed on the top of SU-8 layer 5. Screws are used to tighten the layers together. The assembled tripler is shown in Fig. 9(c).

Photographs of the tripler parts before, during, and after assembly are shown in Fig. 9(d)–(f).

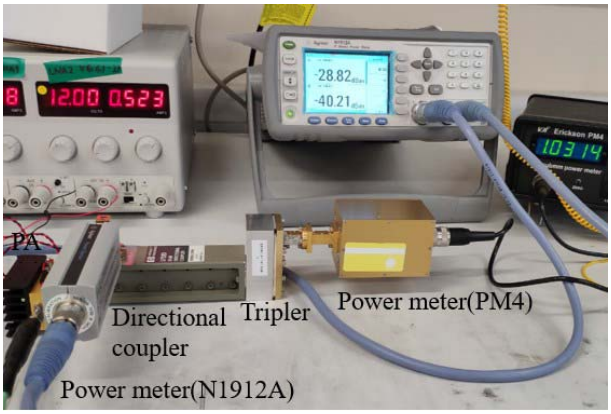

Fig. 10. Tripler measurement setup.

IV. MEASUREMENTS AND DISCUSSION

The measurement setup is shown in Fig. 10. A −20-dB bidirectional coupler was placed at the input of the tripler. The coupler is used to calibrate the input power and to record the input return loss. An Erickson PM4 waveguide power meter was used to measure the output power levels and an Agilent N1912A power meter was used to measure the coupled input or reflected power from the tripler.

For the output power and efficiency measurements, the coupler was connected so that a fraction of the input power was sent to the N1912A power meter. In this configuration, the input and output power can be recorded simultaneously. The input power is first set to sweep from 10 to 80 mW at the center frequency of 47.5 GHz and then set to be 50 mW

TABLE IV
COMPARISON OF SOME MULTIPLIER AND FILTER DESIGNS

Reference	Device type	Waveguide band and Output frequency range	Bandwidth (%)	Input power (mW)	Conversion or Insertion loss Simulated/Measured (dB)	Packaging technique
[15]	Filter	WR-3, 285-315 GHz	9	N/A	N.A/ 1.5-3.5(2.2 on average)	4 layers of SU-8
[27]	Tripler	WR-5, 135-150 GHz	11	50 mW	11-12 / 13-14	CNC split block
[37]	Tripler	WR-1.5, 515-570 GHz	10	100 mW	N.A/18.5-20	DRIE
This work	Tripler	WR-5, 135-150 GHz	11	50 mW	13/ 16-18	5 layers of SU-8

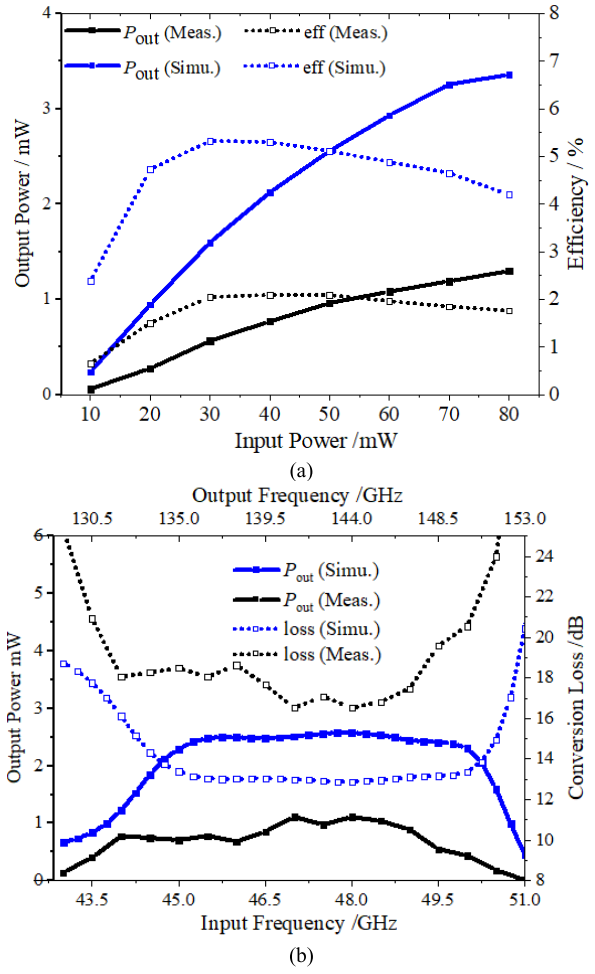

Fig. 11. Simulated and measured tripler performance. (a) Power sweep for 47.5-GHz input frequency. (b) Frequency sweep for fixed 50-mW input power.

(17 dBm) across the 43–51-GHz band. The simulated and measured output power and efficiency for the SU-8 tripler are plotted in Fig. 11. In total, three triplers were fabricated and measured but only the one with the best performance is plotted here. Fig. 11(a) shows the comparison of the measured and predicted output power and efficiency versus input power at a fixed frequency of 47.5 GHz. Maximum power and efficiency of 1.2 mW and 2% were measured, which compares to calculated values of 3.3 mW and 5%, respectively. The simulated and measured efficiency have a similar shape and both peaked at a similar input power of 30–40 mW, suggesting that the diodes are working as expected. The measured conversion loss

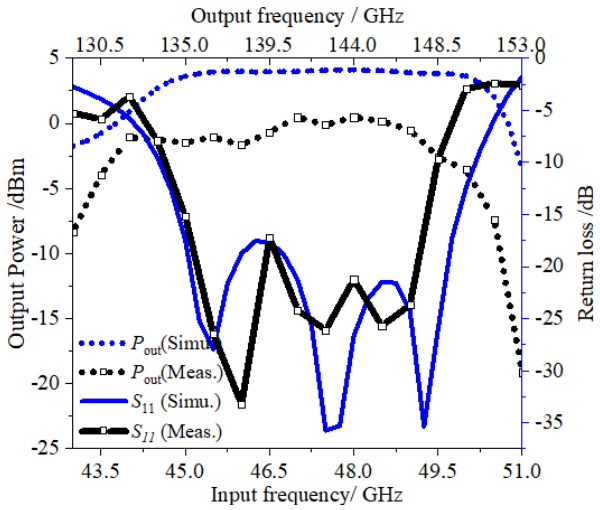

Fig. 12. Simulated and measured tripler output power and return loss across the passband.

is 16–18 dB at the input frequencies of 44–49 GHz for 50-mW input power, as shown in Fig. 11(b).

For the return loss measurement, the directional coupler is connected so the reflected power is coupled to the power meter. In this configuration, the input power is kept constant at 50 mW for all input frequencies. The simulated and measured output power and the tripler input return loss are shown in Fig. 12. There is good agreement for S_{11}, especially for the three reflection poles demonstrating the input filter matching is working well.

As a conclusion, the measured conversion loss for the SU-8 tripler is about 3–5 dB higher than the simulation. Considering the close correlation in the input match measurement and simulation, we believe the difference comes from the following.

1) Additional losses are believed to come from localized air gaps between the layers providing lossy leakage channels. This is exaggerated by small misalignments in the structure and imperfections in the silver film. Such losses, of course, cannot be considered in the simulation.
2) Mismatches at the output port due to the imperfect alignment of the SU-8 layers. From our previous SU-8 work, the typical measured insertion loss for a 9% bandwidth filter can be 1.5–3.5 dB (2.2 dB on average) and, for a 20-mm-long waveguide, another 1-dB loss can be roughly estimated [15].

Although in this work the working frequency is lower, we believe the fabrication of the WR-5 waveguides

(1.296 mm × 0.648 mm) was more challenging compared with the WR-3 waveguides (0.864 mm × 0.432 mm) presented in [15]. The larger waveguide dimensions require one more SU-8 layer, and this becomes more difficult due to additional joints and may result in even higher losses. As discussed in Section III, the assembly of the tripler involves a quartz circuit, and this imposes additional challenges in achieving good alignment between layers. In future works, a double-layer deposition process [15] can be used to joining some of the SU-8 layers or thicker SU-8 layers (e.g., 648 μm instead of 432 μm used in this work) can be used to improve the insertion losses and to simplify the assembly processes.

There is little reported work about micromachined frequency multipliers at similar frequency bands. However, our results are compared with two other multipliers in Table IV. It should be noted that we use the same diode chip and circuit topology as the tripler reported in [27]. Also, a similar packaging technology to that reported in [15] is adopted here. The conversion loss for our SU-8 tripler is 3–4 dB higher than the CNC tripler reported in [27] due to the extra SU-8 waveguide lengths discussed above: bandwidths of all devices are similar.

V. Conclusion

We have presented a WR-5 band biasless frequency tripler based on SU-8 micromachined waveguides. The SU-8 material also serves as the packaging of the Schottky diode MMIC in an MS environment as well as providing the output matching network.

Simulations of the device predict a conversion loss of 13 dB and an input return loss of better than 18 dB. Thermal simulations show the silver-plated SU-8 waveguides with auxiliary thermal paths present a low thermal resistance of 0.18 K/mW. Measurements return an input return loss similar to the simulation and a conversion loss of 16–18 dB, which is 3–5 dB higher than the simulation and 3–4 dB higher than its CNC counterpart. This is mainly due to the higher loss from the output SU-8 filter as well as the extra losses from the 20-mm-long output waveguide.

Although the performance for the presented SU-8 tripler is not as good as its CNC counterpart, we believe it is critical to examine all possible fabrication routes for mm-wave/terahertz components as the small size produces very challenging problems, especially as the frequency increases. It should be noted that micromachining processes have much more potential for smaller and hence higher frequency (>1 THz) waveguides as their size is determined by photolithography rather than a mill tip as in CNC. SU-8 is one such fabrication technique and it is important to have significant work in the area. Further work is expected to improve the losses to that of CNC devices as previously demonstrated for filters. This work demonstrates that waveguides made from multiple layers of SU-8 can be used to package high-frequency active components, in a similar manner to Si-DRIE or LIGA.

References

[1] B. Cheng *et al.*, "340-GHz 3-D imaging radar with 4Tx-16Rx MIMO array," *IEEE Trans. THz Sci. Technol.*, vol. 8, no. 5, pp. 509–519, Sep. 2018.

[2] K. B. Cooper and G. Chattopadhyay, "Submillimeter-wave radar: Solid-state system design and applications," *IEEE Microw. Mag.*, vol. 15, no. 7, pp. 51–67, Nov. 2014.

[3] J. Grajal *et al.*, "Compact radar front-end for an imaging radar at 300 GHz," *IEEE Trans. THz Sci. Technol.*, vol. 7, no. 3, pp. 268–273, May 2017.

[4] H.-J. Song and T. Nagatsuma, "Present and future of terahertz communications," *IEEE Trans. THz Sci. Technol.*, vol. 1, no. 1, pp. 256–263, Sep. 2011.

[5] C. Wang, C. Lin, Q. Chen, B. Lu, X. Deng, and J. Zhang, "A 10-Gbit/s wireless communication link using 16-QAM modulation in 140-GHz band," *IEEE Trans. Microw. Theory Techn.*, vol. 61, no. 7, pp. 2737–2746, Jul. 2013.

[6] J. Treuttel *et al.*, "A 520–620-GHz Schottky receiver front-end for planetary science and remote sensing with 1070 K–1500 K DSB noise temperature at room temperature," *IEEE Trans. THz Sci. Technol.*, vol. 6, no. 1, pp. 148–155, Jan. 2016.

[7] C. Wang and R. Han, "Dual-terahertz-comb spectrometer on CMOS for rapid, wide-range gas detection with absolute specificity," *IEEE J. Solid-State Circuits*, vol. 52, no. 12, pp. 3361–3372, Dec. 2017.

[8] C. Wang, X. Yi, J. Mawdsley, M. Kim, Z. Wang, and R. Han, "An on-chip fully electronic molecular clock based on sub-terahertz rotational spectroscopy," *Nature Electron.*, vol. 1, no. 7, pp. 417–421, Jul. 2018.

[9] B. T. Bulcha *et al.*, "Design and characterization of 1.8–3.2 THz Schottky-based harmonic mixers," *IEEE Trans. THz Sci. Technol.*, vol. 6, no. 5, pp. 737–746, Sep. 2016.

[10] B. Beuerle, J. Campion, U. Shah, and J. Oberhammer, "A very low loss 220–325 GHz silicon micromachined waveguide technology," *IEEE Trans. THz Sci. Technol.*, vol. 8, no. 2, pp. 248–250, Mar. 2018.

[11] J. Hu, S. Liu, Y. Zhang, and R. Xu, "Micromachined terahertz waveguide band-pass filters," in *IEEE MTT-S Int. Microw. Symp. Dig.*, Honolulu, HI, USA, Jun. 2017, pp. 650–653.

[12] J. R. Stanec and N. S. Barker, "Fabrication and integration of micromachined submillimeter-wave circuits," *IEEE Microw. Wireless Compon. Lett.*, vol. 21, no. 8, pp. 409–411, Aug. 2011.

[13] J. W. Digby *et al.*, "Fabrication and characterization of micromachined rectangular waveguide components for use at millimeter-wave and terahertz frequencies," *IEEE Trans. Microw. Theory Techn.*, vol. 48, no. 8, pp. 1293–1302, Aug. 2000.

[14] J.-M. Rollin, D. Miller, M. Urteaga, Z. M. Griffith, and H. Kazemi, "A polystrata 820 mW G-band solid state power amplifier," in *Proc. IEEE Compound Semiconductor Integr. Circuit Symp.*, Oct. 2015, pp. 1–4.

[15] X. Shang, M. Ke, Y. Wang, and M. J. Lancaster, "WR-3 band waveguides and filters fabricated using SU8 photoresist micromachining technology," *IEEE Trans. THz Sci. Technol.*, vol. 2, no. 6, pp. 629–637, Nov. 2012.

[16] H. Yang *et al.*, "WR-3 waveguide bandpass filters fabricated using high precision CNC machining and SU-8 photoresist technology," *IEEE Trans. THz Sci. Technol.*, vol. 8, no. 1, pp. 100–107, Jan. 2018.

[17] Y. Wang, M. Ke, M. J. Lancaster, and J. Chen, "Micromachined 300-GHz SU-8-based slotted waveguide antenna," *IEEE Antennas Wireless Propag. Lett.*, vol. 10, pp. 573–576, 2011.

[18] X. Shang, Y. Tian, M. J. Lancaster, and S. Singh, "A SU8 micromachined WR-1.5 band waveguide filter," *IEEE Microw. Wireless Compon. Lett.*, vol. 23, no. 6, pp. 300–302, Jun. 2013.

[19] X. Shang, H. Yang, D. Glynn, and M. J. Lancaster, "Submillimeter-wave waveguide filters fabricated by SU-8 process and laser micromachining," *IET Microw., Antennas Propag.*, vol. 11, no. 14, pp. 2027–2034, Nov. 2017.

[20] C. E. Collins *et al.*, "A new micro-machined millimeter-wave and terahertz snap-together rectangular waveguide technology," *IEEE Microw. Guided Wave Lett.*, vol. 9, no. 2, pp. 63–65, Feb. 1999.

[21] Y. Li, I. Mehdi, A. Maestrini, R. H. Lin, and J. Papapolymerou, "A broadband 900-GHz silicon micromachined two-anode frequency tripler," *IEEE Trans. Microw. Theory Techn.*, vol. 59, no. 6, pp. 1673–1681, Jun. 2011.

[22] G. Chattopadhayay *et al.*, "Integrated arrays on silicon at terahertz frequencies," in *Proc. IEEE Int. Symp. Antennas Propag.*, Jul. 2011, pp. 3007–3010.

[23] T. Reck *et al.*, "A silicon micromachined eight-pixel transceiver array for submillimeter-wave radar," *IEEE Trans. THz Sci. Technol.*, vol. 5, no. 2, pp. 197–206, Mar. 2015.

[24] G. Chattopadhyay *et al.*, "Compact terahertz instruments for planetary missions," in *Proc. 9th Eur. Conf. Antennas Propag. (EuCAP)*, Lisbon, Portugal, Apr. 2015, pp. 1–4.

[25] W. H. Chow, D. P. Steenson, T. T. Piotrowski, A. Piotrowska, and K. Golaszewska, "An integrated micromachined waveguide frequency tripler for nonlinear wave propagation," in *Proc. IEEE Antennas Propag. Soc. Symp.*, Monterey, CA, USA, Jun. 2004, pp. 1563–1566.
[26] C. Guo *et al.*, "A 290–310 GHz single sideband mixer with integrated waveguide filters," *IEEE Trans. THz Sci. Technol.*, vol. 8, no. 4, pp. 446–454, Jul. 2018.
[27] C. Guo *et al.*, "A 135–150-GHz frequency tripler with waveguide filter matching," *IEEE Trans. Microw. Theory Techn.*, vol. 66, no. 10, pp. 4608–4616, Oct. 2018.
[28] K. Chen, J. Lee, W. J. Chappell, and D. Peroulis, "Co-design of highly efficient power amplifier and high-Q output bandpass filter," *IEEE Trans. Microw. Theory Techn.*, vol. 61, no. 11, pp. 3940–3950, Nov. 2013.
[29] K. Chen, T.-C. Lee, and D. Peroulis, "Co-design of multi-band high-efficiency power amplifier and three-pole high-Q tunable filter," *IEEE Microw. Wireless Compon. Lett.*, vol. 23, no. 12, pp. 647–649, Dec. 2013.
[30] Y. Gao, X. Shang, C. Guo, J. Powell, Y. Wang, and M. J. Lancaster, "Integrated waveguide filter amplifier using the coupling matrix technique," *IEEE Microw. Wireless Compon. Lett.*, vol. 29, no. 4, pp. 267–269, Apr. 2019.
[31] L. Gao, X. Y. Zhang, S. Chen, and Q. Xue, "Compact power amplifier with bandpass response and high efficiency," *IEEE Microw. Wireless Compon. Lett.*, vol. 24, no. 10, pp. 707–709, Oct. 2014.
[32] Q.-Y. Guo, X. Y. Zhang, J.-X. Xu, Y. C. Li, and Q. Xue, "Bandpass class-F power amplifier based on multifunction hybrid cavity–microstrip filter," *IEEE Trans. Circuits Syst. II, Exp. Briefs*, vol. 64, no. 7, pp. 742–746, Jul. 2017.
[33] Y. Gao, J. Powell, X. Shang, and M. J. Lancaster, "Coupling matrix-based design of waveguide filter amplifiers," *IEEE Trans. Microw. Theory Techn.*, vol. 66, no. 12, pp. 5300–5309, Dec. 2018.
[34] J. S. Hong and M. J. Lancaster, *Microstrip Filters for RF/Microwave Applications*. New York, NY, USA: Wiley, 2001.
[35] F. P. Incropera, *Principles of Heat and Mass Transfer*. Hoboken, NJ, USA: Wiley, 2013.
[36] H. Wang, D. Pardo, M. Merritt, N. Brewster, P. G. Huggard, and B. Alderman, "280 GHz frequency multiplied source for meteorological Doppler radar applications," in *Proc. 8th UK, Europe, China Millim. Waves THz Technol. Workshop (UCMMT)*, Cardiff, Wales, Sep. 2015, pp. 1–4.
[37] J. V. Siles *et al.*, "A dual-output 550 GHz frequency tripler featuring ultra-compact silicon micromachining packaging and enhanced power-handling capabilities," in *Proc. Eur. Microw. Conf. (EuMC)*, Paris, France, 2015, p. 84.

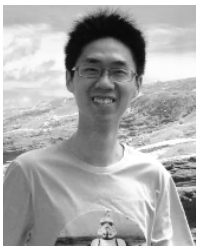

Cheng Guo was born in Chengdu, China, in 1990. He received the B.Eng. degree in communication engineering from Southwest Jiaotong University (Emei Campus), Chengdu, in 2012, and the Ph.D. degree in radio physics from the University of Electronic Science and Technology of China (UESTC), Chengdu, in 2016.

From 2014 to 2016, he was a Visiting Ph.D. Student with the University of Birmingham, Birmingham, U.K., where he was a Research Fellow from 2017 to 2018. He is currently an Associate Professor at the School of Information and Communications Engineering, Xi'an Jiaotong University, Xi'an, China. His current research interests include 3-D printed passive microwave devices, Schottky diode-based THz frequency multipliers and mixers, as well as micromachined mm-wave/THz circuits.

Dr. Guo was a recipient of the IEEE-MTTs Tatsuo Itoh Award in 2017.

Yuvaraj Dhayalan received the M.Sc. degree in materials science from the College of Engineering, Anna University, Chennai, India, in 2004, and the Ph.D. degree from the Indian Institute of Science, Bengaluru, India, in 2010.

He has worked as a Research Fellow with the University of Birmingham, Birmingham, U.K., from 2015 to 2017. He is currently working as a Process Engineer with Huawei Technologies Research and Development, Martlesham, U.K. His research interests are in thin films, nanoscale devices, microfabrication, and nanofabrication.

Xiaobang Shang (M'13–SM'19) was born in Hubei, China, in 1986. He received the B.E. degree (Hons.) in electronics and communication engineering from the University of Birmingham, Birmingham, U.K., in 2008, the B.E. degree in electronics and information engineering from the Huazhong University of Science and Technology, Wuhan, China, in 2008, and the Ph.D. degree in microwave engineering from the University of Birmingham in 2011. His doctoral research concerned micromachined terahertz circuits and the design of multiband filters.

He was a Research Fellow with the University of Birmingham. He is currently a Senior Research Scientist with the National Physical Laboratory (NPL), Middlesex, U.K. His current main research interests include microwave measurements, microwave filters and multiplexers, and micromachining techniques.

Dr. Shang was a recipient of the ARFTG Microwave Measurement Student Fellowship Award in 2009 and a co-recipient of the IEEE Microwave Theory and Techniques Society Tatsuo Itoh Award in 2017.

Jeffrey Powell received the B.Sc. and Ph.D. degrees from the University of Birmingham, Birmingham, U.K., in 1992 and 1995, respectively.

Following graduation, he continued to work at Birmingham, investigating properties of ferroelectric and superconducting materials at microwave frequencies. From 2001 to 2010, he worked as a Principal Engineer with QinetiQ, Bristol, U.K., where he performed many monolithic microwave integrated circuit (MMIC) circuits, hybrid, and module designs for many applications from 2 to 110 GHz using a wide range of commercial and research-based circuit and packaging technologies. In 2010, he formed Skyarna Ltd., a design consultancy that specializes in the design of leading edge circuits, including wideband high-efficiency amplifiers and active circuits to 300 GHz. He has contributed over 50 journals and conference publications and also 2 patent applications.

Michael J. Lancaster (SM'04) was born in York, U.K., in 1958. He received the Ph.D. degree in physics and the Ph.D. degree, with a focus on nonlinear underwater acoustics, from Bath University, Bath, U.K., in 1980 and 1984, respectively.

He joined the Surface Acoustic Wave (SAW) Group, Department of Engineering Science, Oxford University, Oxford, U.K., as a Research Fellow. The research was in the design of new, novel SAW devices, including RF filters and filter banks. In 1987, he became a Lecturer with the Department of Electronics and Electrical Engineering, University of Birmingham, Birmingham, U.K., lecturing in electromagnetic theory and microwave engineering. He began the study of the science and applications of high-temperature superconductors, working mainly at microwave frequencies. He was promoted as the Head of the Emerging Device Technology Research Center, University of Birmingham, in 2000, where he also heads the Department of Electronic, Electrical and Computer Engineering in 2003. He has authored or coauthored 2 books and over 170 articles in refereed journals. His present personal research interests include microwave filters and antennas, as well as the high-frequency properties and applications of a number of novel and diverse materials.

Dr. Lancaster is a Fellow of the IET and the U.K. Institute of Physics. He is a Chartered Engineer and Chartered Physicist. He has served on the MTT IMS technical committee.

Jun Xu was born in Chengdu, China, in 1963. He received the B.S. and M.S. degrees from the University of Electronic Science and Technology of China (UESTC), Chengdu, in 1984 and 1990, respectively.

In 1997, he became an Associate Professor at UESTC and then prompted as a Professor in 2000. His main research interests include microwave theory and technology, millimeter-wave hybrid integrated technology, millimeter-wave communication, and radar radio frequency technology, as well as 3-D printing of passive microwave devices. He is currently the Head of the School of Physical Electronics, UESTC.

Yi Wang (M'09–SM'12) was born in Shandong, China. He received the B.Sc. degree in physics and the M.Sc. degree in condensed matter physics from the University of Science and Technology, Beijing, China, in 1998 and 2001, respectively, and the Ph.D. degree in electronic and electrical engineering from the University of Birmingham, Birmingham, U.K., in 2005.

In 2011, he became a Senior Lecturer and then a Reader at the University of Greenwich, London, U.K. In 2018, he joined the University of Birmingham as a Senior Lecturer. His current research interests include millimeter-wave and terahertz devices for metrology, communications and sensors, micromachining, microwave circuits based on multiport filtering networks, and filter-antenna integration.

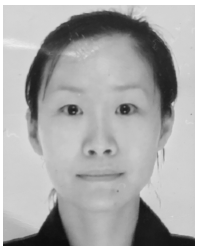

Hui Wang received the M.Sc. and Ph.D. degrees in astrophysics and space instrumentation from the University Pierre and Marie Curie, Paris, France, in 2005 and 2009, respectively.

She joined the Millimeter Wave Technology Group, STFC Rutherford Appleton Laboratory, Oxfordshire, U.K., in 2009, where she is currently leading mixer device development. Her current research interests include millimeter-wave and THz devices, primarily heterodyne frequency mixers, and harmonic up-conversion multipliers, in support of Earth observation and astronomy remote sounding experiments.

Byron Alderman received the M.Phys. degree in physics from the University of Warwick, Coventry, U.K., in 1998, and the Ph.D. degree from the University of Leeds, Leeds, U.K., in 2001.

He joined the Millimeter Wave Technology Group, Rutherford Appleton Laboratory, Oxfordshire, U.K. He founded Teratech Components Ltd., Oxford, U.K., in 2010 and currently the CEO of Teratech and a Principal Scientist at the Rutherford Appleton Laboratory. His research interests are in the field of room temperature heterodyne receiver technology for applications in remote sensing and astronomy at millimeter and submillimeter wavelengths.

Peter G. Huggard (SM'12) received the B.A.(Mod) degree in experimental physics and the Ph.D. degree from the Trinity College, University of Dublin, Dublin, Ireland, in 1986 and 1991, respectively.

He did his postdoctoral research at the University of Regensburg, Regensburg, Germany, and the University of Bath, Bath, U.K. Since 2000, he has been a member of the Millimeter Wave Technology Group, STFC Rutherford Appleton Laboratory, Oxfordshire, U.K. He is currently a U.K. Research Councils Individual Merit Fellow and a Deputy Leader of the Group. He has authored or coauthored over 50 refereed journal articles and a similar number of conference proceedings. His interests include developing photonic sources and semiconductor diode-based receivers for gigahertz and terahertz radiation, the characterization of frequency-selective surfaces, and the calibration of mm-wave radiometers.